PCCP

Cite this: *Phys. Chem. Chem. Phys.*, 2011, **13**, 18038–18046

www.rsc.org/pccp

**PAPER**



# Speciation of uranyl ions in fulvic acid and humic acid: a DFT exploration†

**Mahesh Sundararajan,[a] Gopalan Rajaraman[b] and Swapan K. Ghosh*[ac]**

***Received 19th April 2011, Accepted 19th August 2011***
**DOI: 10.1039/c1cp21238a**

The speciation of uranyl ions in fulvic acid (FA) and humic acid (HA), based on models of larger sizes, is systematically studied using density functional theory (DFT). Four uranyl binding sites are suggested for FA and based on their energetics, the preferential binding sites are proposed. The computed binding sites include two chelating types, one through the carboxylate group and one *via* the hydroxo group. A systematic way to attain the possible structure for Stevenson's HA model is carried out using a combined molecular dynamics (MD) and quantum chemical approach. Calculated structures and energetics reveal many interesting features such as conformational flexibility of HA and binding of hydrophobic molecules in agreement with the experimental suggestions. Five potential binding sites are proposed for uranyl binding to HA and the calculated geometries correlate nicely with the experimental observations. Our binding energy calculations reveal that apart from uranyl binding at the carboxylate functional group, binding at other functional groups such as those involving quinone and hydroxo sites are also possible. Finally, based on our cluster calculations the strength of uranyl binding to HAs and FAs is largely influenced by neighbouring groups *via* hydrogen bonding interactions.

## Introduction

The past fifty years have witnessed many important and exciting developments in the chemistry of actinides. Due to increasing energy demands, actinides are one of the main nuclear energy resources. Besides this, the most well-known utilization of the actinides is in nuclear weapons.[1] Thorium and uranium are used in commercial catalytic systems.[2] Due to radioactive hazards and associated problems, there arise many difficulties in radioactive waste disposal and handling of actinides.[1]

The chemistry of actinides, in particular is receiving increased attention due to the environmental danger posed by such species.[3–6] One possible way to control their release into groundwater is to take advantage of their differing redox behaviour. Strategies for reducing the mobility of these species usually centre on their reduction to less soluble, lower oxidation state species. This process is facilitated by iron containing mineral surfaces,[7] multi-heme cytochromes[8,9] and by humic substances.[10–12]

Humic substances (HSs) are ubiquitous in soils, sediments and natural sources of water. HSs are a complex mixture of organic compounds and may profoundly affect physical, chemical, and biological reactions in the subsurface.[10] Based on the solubility, they can be classified into fulvic acid (FA), humic acid (HA) and Humin. HAs and FAs represent alkali-soluble humus fragments; both FAs and HAs are complex organic compounds, whose X-ray crystal structures are not known. Each fraction of FA and HA must be regarded as made up of a series of molecules of different sizes, few having precisely the same structural configuration or array of reactive groups. It has been generally agreed that both FA and HA contain C, H, O and N elements, although depending on the environment, elements such as sulfur and phosphorous may also be present. FAs are low-molecular weight compounds and possess more O (~40%) content as compared to the high-molecular weight HA (30%). Both FA and HA contain many carboxyl and phenolate functional groups, although carbohydrates and amino acid residues may be found in the latter. In contrast to HAs, FAs contain considerably more functional groups which are acidic in nature. Another important difference is that, while the oxygen in FAs can be accounted for largely in known functional groups (COOH, OH and C=O), a large portion of the oxygen in HAs seems to occur as a structural component of the core (as ether or ester linkages, *etc.*).[10–14]

By combining the data derived from various experimental techniques (EPR, IR, UV-VIS), various structural formulae which are representative of HAs and FAs are proposed,[15–25]

[a] *Theoretical Chemistry Section, Chemistry Group, Bhabha Atomic Research Centre, Mumbai 400 085, India. E-mail: skghosh@barc.gov.in; Fax: +91 22 25505151; Tel: +91 22 25595092*
[b] *Department of Chemistry, Indian Institute of Technology Bombay, Powai, Mumbai 400 076, India*
[c] *Homi Bhabha National Institute, Mumbai 400 094, India*

† Electronic supplementary information (ESI) available: GROMOS FF parameters for HA and binding energy evaluation are given. See DOI: 10.1039/c1cp21238a

 

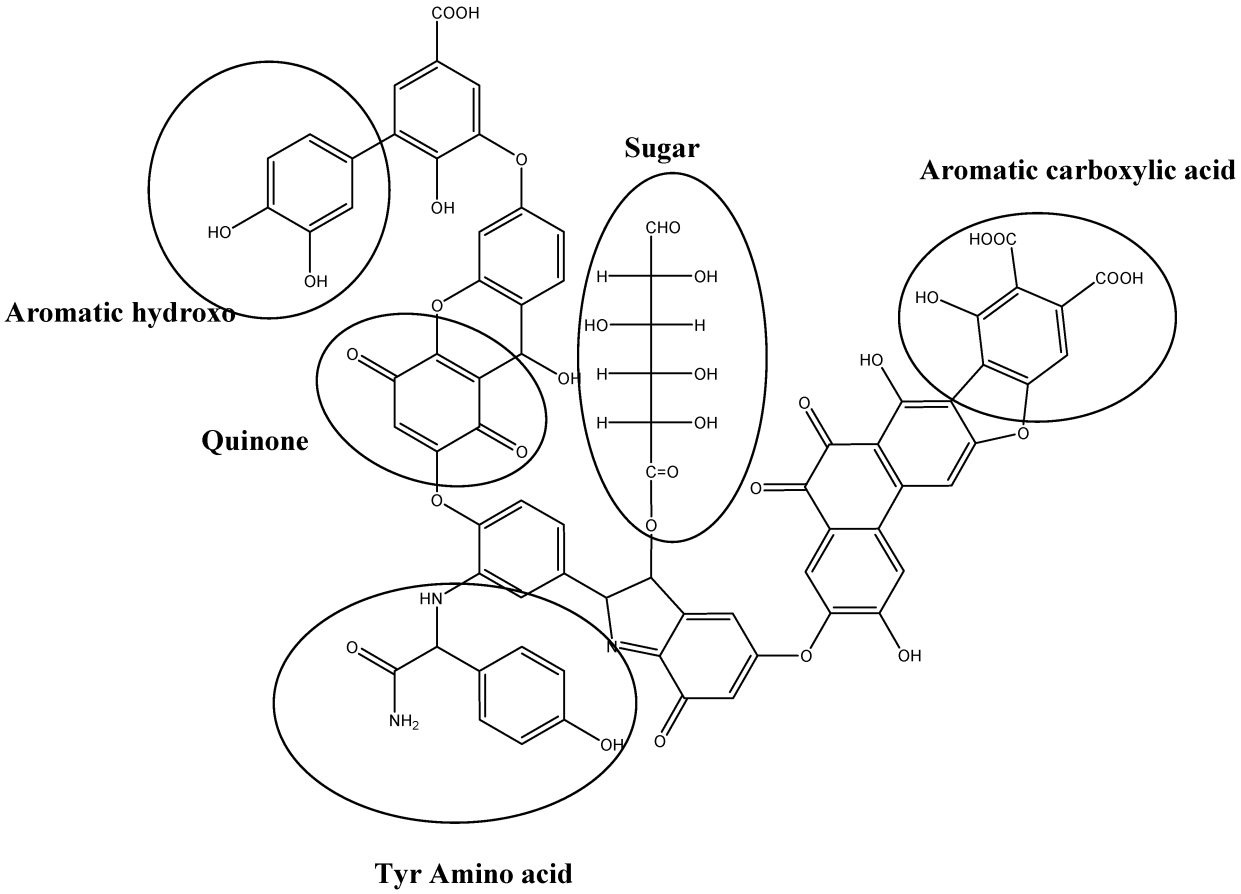


**Fig. 1** Stevenson's proposed structure of HA.

but unfortunately none of the structures proposed are consistent with each other. Stevenson proposed a structural model of HA (Fig. 1), which contains many of the requirements for a typical HA. This includes free and bound phenolic OH groups, quinone moieties, N- and O- atoms as bridging units, aromatic COOH groups, a sugar molecule and an amino acid residue (modeled as tyrosine), thus forming a large organic molecule.[10]

Although the conclusive structural data of HAs and FAs are debatable, the binding affinities of various cations are investigated using various spectroscopic measurements.[26–40] Binding of different metal ions (alkali and alkaline earth metal ions,[31,33] transition[27–30,39] and inner transition metal ions[32]) with varying ionic radii and oxidation states to HAs and FAs has been investigated. It has been thought that carboxylate and phenolate groups were the major binding sites, although other binding motifs cannot be ruled out.[34] Based on the stability constants, it appears that copper ($Cu^{2+}$) binds more strongly as compared to zinc ($Zn^{2+}$).[30] Similarly, tri-valent cations ($Al^{3+}$) have been reported to bind stronger as compared to mono-valent cations ($K^{+}$).[9] Based on the titration experiments, binding of uranyls[34–38,40] and other cations[27–31,33,39] to HA has been reported and tentatively assigned to the carboxylate binding site. Similarly, the complex formations of soil FA for different 3d-transition metal ions have been measured by dialysis titration.[30] Potentiometric and various spectroscopic techniques (IR, UV-VIS) have also been used to understand the uranyl complexation with HAs.[34–38] Here, upon complexation with uranyl, a decrease in carbonyl stretching frequencies was used as a vibrational marker to confirm binding. Xia *et al.* used X-ray absorption spectroscopy to investigate the nature of the binding sites when first row transition elements are bound to aquatic and soil humic substances.[29] Alvarez-Puebla *et al.* investigated the retention mechanism of various first row transition metal di-cations to HA using a combination of physical and chemical techniques.[27]

Computational modelling of HAs and FAs has been limited due to the non-availability of the X-ray structure. However, some preliminary studies on structures and binding of metal ions to models of FA and HA have been reported.[41–53] Here, the flexibility and $Al^{3+}$ cation and benzene interactions to Suwannee FA have been explored using molecular modeling techniques.[52] Conformational searches and minimum energy structure determination have been usually carried out by molecular dynamics (MD) simulations in addition to semi-empirical quantum chemical calculations.[45,46,51,52] Proton binding constants of various clusters of HA models were calculated by Matynia *et al.*[52] Recently, a differential complexation between $Zn^{2+}$ and $Cd^{2+}$ with FA was carried out by Ramalho *et al.* in a density functional theory (DFT) based study.[47] Rösch *et al.* calculated the structures, vibrational frequencies and binding affinities of uranyl(VI) to acetates of aliphatic and aromatic acids and to nitrogen containing complexes.[41–44] Aqueous speciation of uranium, neptunium and plutonium in VI and V

oxidation states of five complexes has been modeled by explicitly incorporating a secondary solvation shell using DFT by Austin *et al.*[49] Further they proposed that among the available density functionals, the M06 suite of density functionals is the method of choice for modeling the actinyls.[50]

In this paper, we report speciation of uranyl ions in FA and HA models and we plan to address the following issues using DFT calculations, *viz*. (i) what are the possible structural models for FAs and HAs, (ii) with the possible structural model in hand, how the HA can be modelled and (iii) what are the possible binding sites of uranyl in FAs and HAs?

## Computational details

### (a) Modelling FA

A realistic description of the electronic structure of FA and HA in aqueous solution requires an appropriate level of a theoretical method based on quantum mechanics (QM) and a proper description of the effect of solvent.

Except for uranyl complexes, all quantum chemical calculations are carried out here using non-relativistic DFT, since high level wavefunction based *ab initio* methods are not practical for systems studied here. However, for metal complexes in particular, there is the ever-present problem of choosing the most appropriate density functional, with both generalized gradient approximation (GGA) and hybrid functionals having been used by several workers. GGA functionals such as BP86 have generally been considered to give the best bond lengths and vibrational frequencies, whilst hybrid functionals such as B3LYP result in better estimates of the energetics.[50,53,54] In the present work, we have used the BP86 functional[55,56] in conjunction with def2-SV(P)[57] basis sets for geometry optimizations. For energetics, the B3LYP functional[58,59] in conjunction with TZVP basis sets[60,61] are utilized as implemented in TURBOMOLE.[62] For uranyl complexes, geometry optimizations were carried out using def-ECP pseudopotential and def-SV(P) basis sets to treat the core and valence electrons. For the corresponding energetics, ECP-60-MWB and def-TZVP basis sets were used. For both geometries and energetics, solvent effects were incorporated *via* the COSMO continuum model as implemented in TURBOMOLE program package. Minimum energy structures of FA–uranyl complexes were characterized as minima by carrying out harmonic frequency calculations. We have tested the sensitivity of uranyl binding energies to FA when the M06 functional[63] is used. M06 calculations were carried out using Gaussian 09 programs[64] within the C-PCM continuum solvation model.

### (b) Modelling HA

The structure of HA has been modelled by a cost effective approach as follows. We have opted to use a combined classical MD and DFT method, which has been known to give reliable results comparable with *ab initio* Car–Parrinello MD simulations (CPMD).[49] The GAUSSVIEW 03 program was employed as a graphical interface for the construction and visualization of the molecular structure of HA as proposed by Stevenson[10] (Fig. 1). In our model, the amino acid residue has been modeled as a tyrosine residue (Tyr). Geometry optimization of this structure (160 atoms) has been carried out using the BP86 functional in conjunction with def2-SV(P) basis sets. As there are no standard force field parameters available for Stevenson's HA model, we have generated the GROMOS-96 force field parameters[65,66] using the pro-drg2.5 program.[67] Furthermore, the charges derived by pro-drg2.5 were modified by calculating more accurate electrostatic potential derived charges (BP86/def2-SV(P)) using CHELPG algorithm[68] as implemented in ORCA[69] (BP86/SV(P)). Preliminary calculations were performed to check the parameters and no severe distortions such as bond breaking have been noticed. The resulting HA structure is solvated by a large number of water molecules. The initial structure is of charge equal to four units and correspondingly four sodium ions were added to neutralize the system. This model structure was optimized by minimizing the energy using the steepest descent algorithm. The optimized geometry is then equilibrated by performing classical Molecular Dynamics (MD) simulations for 10 ns using GROMACS MM package.[70] Trajectories generated after every one nanosecond were then used for subsequent geometry optimizations (BP86/def2-SV(P)) to identify the global minimum energy structure within the timescale. For DFT optimizations, the box solvent water molecules were neglected and the solvent effects are subsequently modelled using the COSMO continuum solvation model. The energies were again evaluated using the B3LYP/TZVP basis set. The lowest energy structure was used for uranyl complexation at different binding sites.

## Results and discussion

### (a) Uranyl ion complexation with FA

We have considered here a FA model reported by Wang *et al.*[14] (Fig. 2), with the chosen structure having the essential features for binding metal ions. The chosen model consists of substituted pyran rings, catecholate, quinone and carboxylate functional groups which are potential binding sites for metal ions. DFT optimized bond lengths (BP86/def2-SV(P)) of FA of Wang's model are found to be in excellent agreement with the available X-ray data[14] (Fig. 2). Due to strong hydrogen bonding, the optimized structure of FA is planar which is consistent with the X-ray data reported[14] and the optimized structure is characterized as minima. From the calculated IR-spectrum, it is possible to assign the values of vibrational

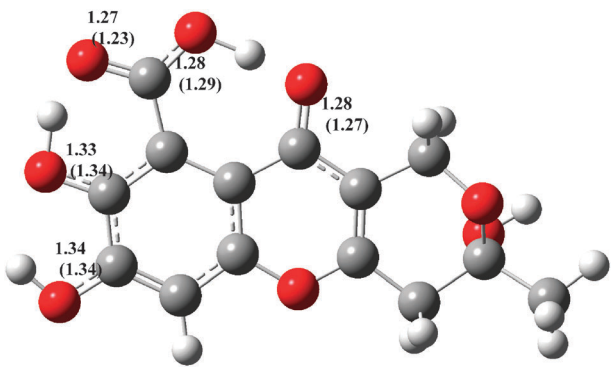


**Fig. 2** Optimized structure (Å) of FA. Values in parentheses denote X-ray data.[14]

 

frequencies in the range 3400–3350 $cm^{-1}$ to O–H stretching, 3000–2900 $cm^{-1}$ to C–H stretching in $CH_2$ and $CH_3$ groups. A characteristic peak at 1730 $cm^{-1}$ can be attributed to carbonyl stretching in $COO^-$ groups, 1650 $cm^{-1}$ to anti-symmetric O–C–O bond vibrations in $COO^-$ groups or to aromatic C=C stretching. Finally, a peak at 1560 $cm^{-1}$ can be assigned to aromatic C=C stretching and C=O stretching. The calculated IR spectrum is consistent with the experimental data of other FAs and provides confidence on the chosen model and theoretical levels for the calculation of the FA structure.[34]

We have identified four possible binding sites in FA (Fig. 3). Deprotonation of the carboxylate group produces two binding sites denoted as FA-1 and FA-2 in Fig. 3. In FA-1, oxygen atoms of carboxylate and quinone functional groups coordinate to uranyl ions, whereas in FA-2, both the carboxylate oxygens can coordinate *via* the bidentate motif. Deprotonation of the hydroxo-group can lead to the formation of a binding site denoted as FA-3. At this binding site, the uranyl ion forms a chelate complex by coordinating to a hydroxo oxygen and a carboxylate oxygen. Finally, removal of two protons from two hydroxo groups leads to the fourth binding site (FA-4) where both phenoxide ions can coordinate to uranyl.

Before we discuss the uranyl–FA complexes, we shall glance through the optimized structure of FA binding sites. In all four binding sites, the planarity of the molecule is lost due to the absence of intra-molecular hydrogen bonding. Of the four complexes, FA-3 is the most stable species and FA-4 is the least. Hence, the binding energies are calculated with the lowest energy FA-3 ligand (Table 1). All the four binding sites were characterized as minima by carrying out harmonic frequency calculations.

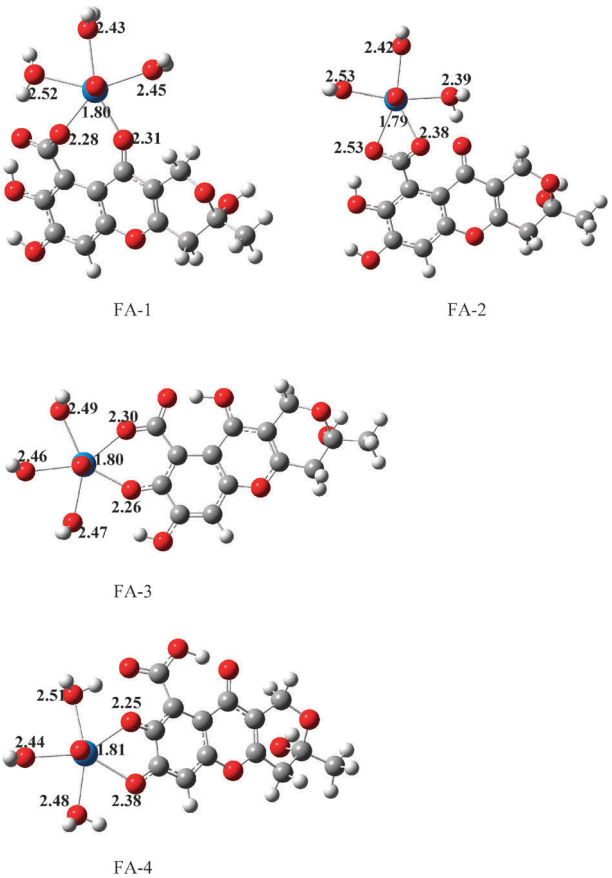


**Fig. 3** Optimized uranyl bound fulvic acid structures (Å).

Finally, we believe that the inner sphere complexes of uranyl with FA are formed in an aqueous environment, where the FA ligand displaces two equatorial waters of the penta-aquo uranyl complex. For comparison, in Table 1, we have also given the geometric parameters of the hydrated uranyl complex. In fact, the calculated geometry and vibrational spectra of the penta-aquo uranyl complex ($[UO_2(H_2O)_5]^{2+}$) are found to be consistent with earlier predictions and with experimental data.[49]

Compared to the penta-aquo uranyl complex, the U=O bond lengths are slightly elongated when the uranyl ion is complexed with FA at all four binding sites. This is due to the stronger binding of the negatively charged FA with the positively charged uranyl ion *via* ion–dipole interaction. The introduction of an asymmetric ligand (FA) leads to a distortion in the coordination of equatorial water molecules to the uranyl moiety.

When a uranyl ion is attached to FA-1, one of the three water molecules bound to uranyl is hydrogen bonded to the carboxylate oxygen (1.87 Å) of the FA ligand and hence a corresponding elongation of the uranyl–water bond length is noted (2.52 Å). However, for the other two water molecules, no such hydrogen bonding is present and hence the binding to the uranyl ion is stronger (~2.44 Å). The charge on carboxylate oxygen (−0.413 $e^-$) is somewhat larger as compared to quinone oxygen (−0.403 $e^-$). Hence, as compared to quinone oxygen, the carboxylate–uranyl bond length (2.28 Å) is slightly shorter.

In FA-2, a water molecule bound to uranyl is hydrogen bonded to the neighbouring oxygen of FA, but unlike in FA-1, it now interacts with the quinone oxygen atom of FA (1.59 Å). The coordination mode of carboxylate to uranyl is asymmetric (2.38 Å and 2.53 Å) due to differing charges on the two oxygens (−0.413 $e^-$ and −0.347 $e^-$). The calculated structural parameters can be compared with those of a uranyl benzoate molecule for which experimental data are available.[71] Our optimized structure for the U=O bond length (1.79 Å) is very close to the experimental result (Table 1). However the optimized uranyl carbon bond length is somewhat shorter by ~0.1 Å as compared to the experimental data. Such a reduction in the U–C bond length has also been noted in the DFT calculations of a uranyl–benzoate molecule by Rösch *et al.*[42]

In FA-3, we do not find any significant hydrogen bonding interactions present between the uranyl bound water molecules and the FA ligand. In comparison to the carboxylate oxygen–uranyl bond, phenoxide–uranyl is slightly stronger (0.04 Å) which can again be attributed to the differing charges on phenoxide oxygen (−0.499 $e^-$) and carboxylate oxygen (−0.416 $e^-$). Finally in FA-4, asymmetric binding of two phenoxide oxygens to uranyl is observed. In this species, two bound water molecules are hydrogen bonded with the coordinating phenoxide oxygen atoms (2.20 Å, 2.28 Å) and to carboxylate oxygen (1.62 Å) of FA. Due to these additional interactions, water coordination to uranyl becomes weak (Fig. 3, Table 1).

**Table 1** Optimized structural parameters (Å), vibrational frequencies ($cm^{-1}$) and binding energies (kcal $mol^{-1}$) of uranyl ions coordinated to FA at different binding pockets

| | Bond length/Å | | | Vibrational frequencies/$cm^{-1}$ | | |
|---|---|---|---|---|---|---|
| | U–O | Calculated | Experiment[49,71] | Calculated | Experiment[49,71] | Calculated binding energy |
| $([UO_2(H_2O)_5]^{2+}$ | U═O | 1.78 | 1.76–1.78 | $\nu_{sym}$ = 889 | $\nu_{sym}$ = 870 | — |
| | $U–O_{H_2O}$ | 2.42 | 2.41–2.45 | $\nu_{asym}$ = 984 | $\nu_{asym}$ = 964 | |
| FA-1 | U═O | 1.80 | — | $\nu_{sym}$ = 809 | — | −23.0 |
| | $U–O_{FA}$ | 2.28–2.31 | | $\nu_{asym}$ = 884 | | |
| | $U–O_{H_2O}$ | 2.43, 2.45, 2.52 | | | | |
| FA-2 | U═O | 1.79 | 1.77–1.78 | $\nu_{sym}$ = 830 | $\nu_{sym}$ = 847 | −13.1 |
| | $U–O_{FA}$ | 2.38, 2.53 | 2.41–2.43 | $\nu_{asym}$ = 903 | $\nu_{asym}$ = 931–934 | |
| | $U–O_{H_2O}$ | 2.39–2.42 | — | | | |
| | U–C | 2.79 | 2.88–2.91 | | | |
| FA-3 | U═O | 1.80 | — | $\nu_{sym}$ = 805 | — | −25.8 |
| | $U–O_{FA}$ | 2.26–2.30 | | $\nu_{asym}$ = 881 | | |
| | $U–O_{H_2O}$ | 2.46–2.49 | | | | |
| FA-4 | U═O | 1.81 | — | $\nu_{sym}$ = 787 | — | +6.6 |
| | $U–O_{FA}$ | 2.25, 2.38 | | $\nu_{asym}$ = 864 | | |
| | $U–O_{H_2O}$ | 2.44, 2.48, 2.51 | | | | |

Upon uranyl binding to FA, significant charge transfer from FA to $[UO_2]^{2+}$ takes place. In comparison to the fully hydrated uranyl complex, all four binding sites reduce the positive charge at the uranium centre and a corresponding increase in the negative charge on axial oxygen of the uranyl moiety leading to an elongation of the U═O bond length. Of the two binding sites, charge transfer at FA-4 is largely due to the di-anionic nature of FA prior to binding.

The experimental vibrational frequencies for the uranyl complex of FA relate mainly to the asymmetric U═O modes. We were able to identify both symmetric ($\nu_{sym}$) and asymmetric ($\nu_{asym}$) modes from our calculations (Table 1). Experimentally 847 $cm^{-1}$ for $\nu_{sym}$ and 931–934 $cm^{-1}$ for $\nu_{asym}$ have been reported. For the computed structures FA-1 to FA-4 the $\nu_{sym}$ varies from 787 to 830 $cm^{-1}$ while the $\nu_{asym}$ varies from 864 to 903 $cm^{-1}$. Generally the spectra reflect the differing bond length patterns present in the four complexes. Hence, of the four complexes, both $\nu_{sym}$ and $\nu_{asym}$ stretching are strongest for FA-2 as compared to other three binding sites, with the same for FA-4 being the weakest.

The calculated uranyl binding energies (refer ESI†) to FA are as follows, FA-3 > FA-1 > FA-2, whereas binding at the FA-4 site is found to be unfavourable. For FA-3 and FA-1 binding sites, the calculated binding energies are significant (~25 kcal $mol^{-1}$) as compared to FA-2 (13 kcal $mol^{-1}$).

The difference in binding energies arises from ligand stabilization energies. FA-3 is the most stable species prior to uranyl binding and hence the uranyl binding is maximum.

Finally, we have also computed the binding energies using the M06 functional and compared them with the results based on the B3LYP functional. The calculated binding energies are slightly modified (by less than 1 kcal $mol^{-1}$) when the M06 functional in conjunction with TZVP basis sets was used. In the forthcoming sections, we will discuss the structures and binding affinities in HA and compare with those of FAs.

The binding affinity of uranyl at the respective binding site depends on the ability of the ligand to donate negative charge to the uranyl moiety. The binding nature and donation of a U–O (donor) bond vary from FA-1 to FA-4 structures. The FA-1 structure forms a seven membered chelation upon binding uranium while FA-2 has only a three membered ring, whereas both FA-3 and FA-4 have six membered chelation. Since the uranium atom is in VI oxidation state with a very high positive charge on it, the newly forming U–O (donor) bonds are formed by donation of electrons from oxygens of FA to the empty orbitals of uranium, especially to the 7s, 5f and 6d orbitals. Since the computed binding energies are related to the bonding, we have plotted one of the frontier orbitals present in FA-1 to FA-4 where this $O(p_y)$–U(f) bonding interaction has been detected. It's apparent from these orbital plots that FA-3 (also FA-4 but the nature of the f-orbital varies here) has strong interaction with the f-orbitals of the uranium while in FA-2, the orbitals are close lying and have net anti-bonding character.

### (b) Conformational flexibility of the HA model

In Fig. 4, we have shown the relative energies (evaluated at B3LYP/TZVP) of HA structures obtained at different timescales of MD simulations. The positions of the binding sites are significantly modified during the course of the simulations. For instance, the hydrophilic residues such as carboxylates, phenoxide, quinones and sugar molecules are involved in hydrogen bonding. Indeed, our calculations do show that HA is a flexible molecule and can adopt various conformations and inter-conversion from one to another is energetically feasible.[11,72] Of the eleven structures computed, the DFT optimized structure at 5 ns is found to be the most stable structure (Fig. 5).

We find that in our 10 ns simulations, the sugar molecule and tyrosine amino acid residues are one of the flexible entities which can change the conformation of HA *via* hydrogen bonding. On one side, a flexible highly substituted biphenyl ring is present and on the other side, a rigid substituted heterocyclic ring system is present. Hence the major conformational changes in HA should arise from the interactions with the three flexible (sugar, tyrosine and substituted biphenyl ring) parts. Any severe distortion in the aromatic ring systems should lead to high energy species. Indeed, DFT optimized structures at 1 ns, 6 ns and 9 ns are such high energy species. However, we find

 

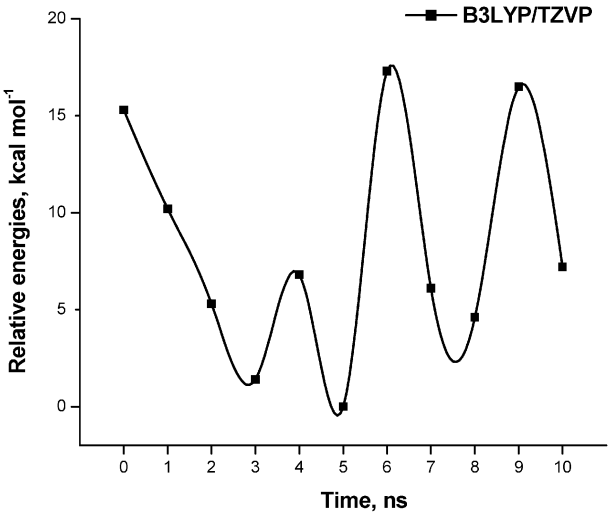


**Fig. 4** Relative energies (kcal $mol^{-1}$) evaluated using B3LYP/TZVP of different HA structures generated during the course of 10 ns MD simulations.

that for structures at 3 ns, 5 ns, 7 ns and 8 ns, a strong and favourable electrostatic interaction between the three flexible portions of the molecules of variable strengths is clearly seen. The DFT optimized 5 ns structure possesses a cyclic ring like structure at one end, stabilized largely by hydrogen bonding interactions with the three flexible molecules. It is known that such a cyclic structure is one of the possible structures of HA, which can trap many cations and organic molecules. Further, our calculations suggest that more than six structures are possible within a 10 kcal $mol^{-1}$ energy margin, and hence depending on the environmental conditions, a wide variety of conformations can be adopted by HA.[11,72] Nevertheless, we have taken the lowest energy conformer and studied the complexation behaviour of uranyl at different binding sites.

### (c) Uranyl ion complexation with HA

We now present our results on possible structures for binding affinities of uranyl at various binding pockets of the most stable HA structure (5 ns). Due to multiple binding sites, choice of the binding sites is based on p$K_a$ calculations carried out using PM6 Hamiltonian.[73] Replacement of an acidic proton by a uranyl complex creates two binding pockets (denoted as HA-1 and HA-2), whereas binding at the carboxylate leads to two more binding sites (denoted as HA-3 and HA-5). Finally the binding of uranyl at the 1,2-benzoquinone position leads to HA-4 (Fig. 5). Prior to uranyl binding to HA, we noticed that HA-3 is the most stable structure as compared to HA-1 and HA-2.

Compared to uranyl hydrated species, slightly longer U═$O_{yl}$ and U–$O_{H_2O}$ bond lengths are noted for all five uranyl–humate complexes (Table 2, Fig. 6). Except in HA-3 and HA-5, asymmetric binding of HA to uranyl is noted. Further, the U═$O_{yl}$ bond lengths are very similar for all five binding sites. In all the five optimized structures, the Tyr residue and the sugar molecule are strongly hydrogen bonded with the quinone molecule such that a cyclic structure is formed at one end of HA (Fig. 5).

In the HA-1 binding site (Fig. 6, Table 2), the water molecule bound to uranyl is involved in hydrogen bonding with the neighbouring HA residues leading to elongated U–$O_{H_2O}$ bond lengths. The quinone oxygen interaction with uranyl is somewhat stronger (2.29 Å) as compared to the phenoxide ion (2.38 Å). By replacement of a proton at 5-hydroxy-1,2-naphthoquinone, uranyl is found to be coordinated by a phenoxide ion and quinone oxygen (HA-2). The coordinating phenoxide ion is hydrogen bonded by the neighbouring substituted phenol moiety which abstracts some charges, leading to weaker binding to uranyl (2.37 Å) as compared to the naphthoquinone (2.30 Å) moiety (Fig. 6, Table 2). Further, the coordinated water molecule is now hydrogen bonded with the neighbouring hydroxo-group.

Before discussing the carboxylate binding to HA (HA-3 and HA-5), we now discuss the binding of uranyl at the 1,2-benzoquinone moiety (HA-4). Similar to HA-2, the coordinating quinone oxygens are hydrogen bonded by neighbouring hydroxyl protons and the coordinating water molecules are hydrogen bonded to the humate hydroxo-group (Fig. 6). These variances in geometry lead to the asymmetric binding of quinone oxygens to uranyl. Compared to other complexes, the binding of quinone oxygens to uranyl is somewhat weak (Table 2) and a corresponding reduction in U–$O_{H_2O}$ bond lengths is noted.

Unlike the above three binding sites and those of FA-2 complexes, a symmetric binding of carboxylate to uranyl is noticed for both HA-3 (2.40 Å) and HA-5 (2.37 Å). This binding is expected as carboxylate functional groups at the terminal positions are not involved in any hydrogen bonding within HA. Based on uranyl–carboxylate bond lengths, HA-3 is considered to be somewhat weakly bound as compared to HA-5 (Fig. 6).

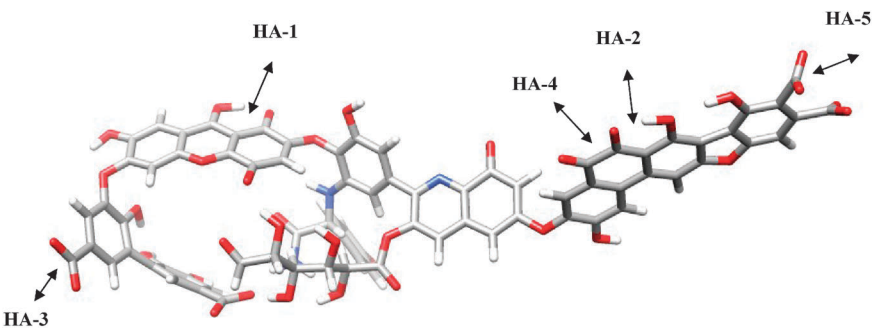


**Fig. 5** DFT optimized structure of a 5 ns structure generated from classical MD simulations. Five possible binding sites are shown.

**Table 2** Optimized structural parameters (Å) and binding energies (kcal mol$^{-1}$) of uranyl ions coordinated to HA at different binding pockets

| | | Bond length/Å | | |
|---|---|---|---|---|
| | | Calculated | Experiment[37,74,75] | Calculated binding energy |
| HA-1 | X═O | 1.81 | 1.77–1.78 (0.02) | +8.1 |
| | $X–O_{HA}$ | 2.29, 2.38 | — | |
| | $X–O_{H_2O}$ | 2.45–2.47 | 2.38–2.40 (0.02) | |
| | U–C | 3.41, 3.45 | | |
| HA-2 | X═O | 1.80 | 1.77–1.78 (0.02) | +11.3 |
| | $X–O_{HA}$ | 2.30, 2.37 | — | |
| | $X–O_{H_2O}$ | 2.45–2.47 | 2.38–2.40 (0.02) | |
| | U–C | 3.42, 3.47 | | |
| HA-3 | X═O | 1.80 | 1.77–1.78 (0.02) | −26.3 |
| | $X–O_{HA}$ | 2.40 | — | |
| | $X–O_{H_2O}$ | 2.43 | 2.38–2.40 (0.02) | |
| | U–C | 2.80 | | |
| HA-4 | X═O | 1.80 | 1.77–1.78 (0.02) | −8.9 |
| | $X–O_{HA}$ | 2.37, 2.47 | — | |
| | $X–O_{H_2O}$ | 2.42–2.43 | 2.38–2.40 (0.02) | |
| | U–C | 3.28, 3.32 | | |
| HA-5 | X═O | 1.80 | 1.77–1.78 (0.02) | −29.3 |
| | $X–O_{HA}$ | 2.36, 2.37 | — | |
| | $X–O_{H_2O}$ | 2.43–2.44 | 2.38–2.40 (0.02) | |
| | U–C | 2.77 | | |

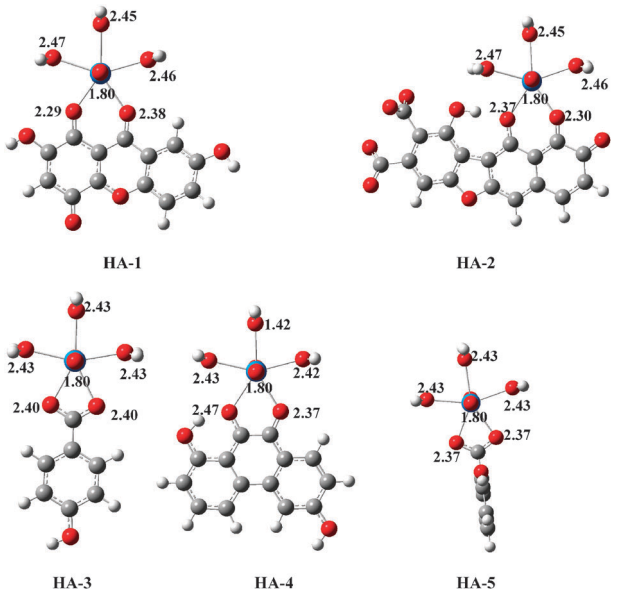


**Fig. 6** Important structural parameters (Å) of uranyl binding at five different HA sites. Only the neighboring environments are shown for clarity.

We can compare the optimized bond lengths with the corresponding experimental data for uranyl–HA complexes.[37,74,75] The calculated U–C bond length (2.77 Å for HA-3 and 2.80 Å for HA-5) is close to the experimental result for the uranyl benzoate complex (2.88 Å). For the other three complexes (HA-1, HA-2 and HA-4), this value is more than 3.25 Å. Due to the large size of HA–uranyl complexes (175 atoms), we were unable to compute vibrational frequencies. The computed binding energies are reported in Table 2. Our calculations at the B3LYP/TZVP level predict two weak and three strong binding sites. Binding of uranyl at HA-1 and HA-2 is unfavourable, whereas for other three sites, it is strong. Compared to HA-3 and HA-5, the uranyl binding to the HA-4 binding site is weak perhaps due to the lack of charge transfer from HA to uranyl. The lack of negative charge on this centre can be attributed to aromaticity. Uranyl coordination at the HA-4 binding site does not possess an aromatic benzene ring and hence lacks the ability for the bound oxygen to donate electrons to uranyl. However, for HA-3 and HA-5 carboxylate groups are bound to aromatic phenyl rings. Unlike the carboxylate–uranyl complex in FA-2, for the carboxylate–uranyl complexes in HA models (HA-3 and HA-5), the binding energies are stronger.[35] The calculated binding energies of HA-3 and HA-5 are somewhat larger (4–8 kcal mol$^{-1}$) as compared to those of uranyl–benzoate complexes computed by Rösch *et al.*[42]

Based on Raman spectroscopy, it was reported that in addition to carboxylate binding, chelate type binding is also possible. In fact, the symmetric stretching for a salicylate complex is downshifted as compared to oxalate and malonate complexes.[38] Our findings are in line with these experimental observations suggesting that both chelate type (HA-4)[34] and carboxylate type bindings (HA-3 and HA-5) are indeed feasible.

## Conclusions

Understanding the behaviour of heavy metal ions in various environments has attracted attention in recent years due to their relevance to present day energy crisis. It is long known that HAs and FAs are potential binders of uranyl. Some structural studies and p$K_a$ evaluation studies based on small models were proposed earlier. In fact, except that of Rösch *et al.*,[41–44] no quantum chemical calculations were performed on the behaviour of uranyl binding to HA models. Hence, in this paper, we have presented a systematic and thorough study of uranyl binding to FA and HA using models of larger sizes (more than 160 atoms) proposed by Wang *et al.*[14] and Stevenson.[10] To our knowledge, our calculation is the first study of uranyl binding to multiple binding sites present within the models of FAs and HAs. The main conclusions that can be drawn from our work are as follows:

 

(a) The calculated vibrational frequencies for Wang's FA model are close to those of vibrational frequencies estimated for naturally occurring FA structures. The agreement between the experiment and calculated results reveals that our FA structure is likely to be close to the real structure and it possesses carboxylates, hydroxo and quinone functional groups which are potential uranyl binders.

(b) Our DFT based calculations suggest that uranyl binding is strongly favourable at three FA sites (FA-1 to FA-3), whereas, binding at the hydroxo group (as in FA-4) is unfavourable as evident from the binding energy ($\sim$7 kcal mol$^{-1}$).

(c) Our combined MD-DFT studies confirm the flexibility of the HAs reported earlier in the experimental studies. Further, we have revealed five binding sites of which uranyl binding to carboxylate functional groups (HA-3 and HA-5) are favoured over the other binding sites by more than 15 kcal mol$^{-1}$. Other binding sites which do not possess aromaticity such as quinone functional groups (HA-1 and HA-2) are endothermic in nature and are thus highly unlikely to be involved in uranyl binding.

(d) In our chosen models of FA and HA, we find that the uranyl binding sites typically possess aromatic carboxylates, quinone, hydroxo functional groups. The binding energies for strongly favourable sites are of the order of $\sim$23 kcal mol$^{-1}$ in both FA and HA models.

Despite this extensive study, the proposed structures have some limitations. For example our proposed structure for HA can be criticized for not having functional groups involving sulfur and phosphorus atoms. Additionally, in our models the carboxylate groups are deprotonated while the phenolic groups remain protonated. The penta-aquo uranyl complex may dominate in solutions which are acidic (low pH). It is known that HA is sensitive to varying pH conditions and ionic strengths and calculations in this direction are in progress in our laboratory.[40]

## Acknowledgements

MS and SKG thank KSKRA fellowship for funding and Dr T. Mukherjee for his kind support and the BARC computer center for providing the high performance parallel computing facility (Ameya and Ajeya Systems). Funding from the INDO-EU project MONAMI is also gratefully acknowledged. GR would like to gratefully acknowledge financial support from the Government of India through Department of Science and Technology (SR/S1/IC-41/2010) and computational resources at Indian Institute of Technology Bombay.

## References

1 J. J. Katz, G. T. Seaborg and L. R. Morss, *The Chemistry of the Actinides*, Chapman & Hall, London, 2nd edn, 1986.
2 A. Andrea, E. Barnea and M. S. Eisen, *J. Am. Chem. Soc.*, 2008, **130**, 2454.
3 R. T. Anderson, H. A. Vrionis, I. Ortiz-Bernad, C. T. Resch, P. E. Long, R. Dayvault, K. Karp, S. Marutzky, D. R. Metzler, A. Peacock, D. C. White, M. Lowe and D. R. Lovley, *Appl. Environ. Microbiol.*, 2003, **69**, 5884.
4 D. R. Lovley, E. J. P. Phillips, Y. A. Gorby and E. Landa, *Nature*, 1991, **350**, 413.
5 D. R. Lovley, E. E. Roden, E. J. P. Phillips and J. C. Woodward, *Mar. Geol.*, 1993, **113**, 41.
6 G. R. Choppin, *J. Radioanal. Nucl. Chem.*, 2007, **273**, 695.
7 A. L. Neal, J. E. Amonette, B. M. Peyton and G. G. Geesey, *Environ. Sci. Technol.*, 2004, **38**, 3019.
8 M. Assfalg, I. Bertini, M. Bruschi, C. Michel and P. Turano, *Proc. Natl. Acad. Sci. U. S. A.*, 2002, **99**, 9750.
9 J. C. Renshaw, L. J. C. Butchins, F. R. Livens, I. May, J. M. Charnock and J. R. Lloyd, *Environ. Sci. Technol.*, 2005, **39**, 5657.
10 F. J. Stevenson, *Humus Chemistry: Genesis, Composition, Reactions*, John Wiley & Sons, New York, 1994.
11 E. A. Ghabbour and G. Davies, *Humic Substances: Structures, Models and Functions*, RSC publishing, Cambridge, UK, 2001.
12 I. H. Suffer, and P. MacCarthy, *Aquatic Humic Substances: Influence on Fate and Treatment of Pollutants*, ACS, Washington, 1989.
13 E. M. Pena-Mendez, J. Havel and J. Patocka, *J. Appl. Biomed.*, 2005, **3**, 13.
14 J. F. Wang, M. F. Fang, H. Q. Huang, G. L. Li, W. J. Su and Y. F. Zhao, *Acta Crystallogr., Sect. E: Struct. Rep. Online*, 2003, **E59**, o1517.
15 A. Jezierski, F. Czechowski and D. Jerzykiewicz, *Appl. Magn. Reson.*, 2000, **18**, 127.
16 R. Khanna, M. Witt, M. K. Anwer, S. P. Agarwal and B. P. Koch, *Org. Geochem.*, 2008, **39**, 1719.
17 I. V. Perminova, N. Y. Grenhishcheva and V. S. Petrosyan, *Environ. Sci. Technol.*, 1999, **33**, 3781.
18 J. A. Leenheer, R. L. Wershaw and M. M. Reddy, *Environ. Sci. Technol.*, 1995, **29**, 399.
19 W. Fuchs, *Kolloid-Z.*, 1930, **52**, 248.
20 W. Fuchs, *Die Chemie der Kohle*, Springer, Berlin, 1931.
21 M. Kononova, *Soil Organic Matter*, Pergamon, London, 1966.
22 W. Flaig, *Suom. Kemistil. A*, 1965, **A33**, 229.
23 G. T. Felbeck Jr, *Adv. Agron.*, 1965, **17**, 327.
24 M. Schnitzer and S. U. Khan, *Humic Substances in the Environment*, Marcel Dekker, New York, 1972.
25 J. A. E. Buffle, *Conference Proceedings de la Commission d'Hydrologie Appliquee de l' A. G. H. T. M.*, University of Orsay, 1977, pp. 3–10.
26 J. J. Lenhart, S. E. Cabaniss, P. MacCarthy and B. D. Honeyman, *Radiochim. Acta*, 2000, **88**, 345.
27 R. A. Alvarez-Puebla, C. Valenzuela-Calahorro and J. Garrido, *Langmuir*, 2004, **20**, 3657.
28 T. J. Strathmann and S. C. B. Myneni, *Geochim. Cosmochim. Acta*, 2004, **68**, 3441.
29 K. Xia, W. Bleam and P. A. Helmke, *Geochim. Cosmochim. Acta*, 1997, **11**, 2223.
30 D. P. Rainville and J. H. Weber, *Can. J. Chem.*, 1982, **60**, 1.
31 C. David, S. Mongin, C. Rey-Castro, J. Galceran, E. Companys, J. L. Garces, J. Salvador, J. Puy, J. Cecilla, P. Lodeiro and F. Mas, *Geochim. Cosmochim. Acta*, 2010, **74**, 5216.
32 A. J. Peters, J. Hamilton-Taylor and E. Tipping, *Environ. Sci. Technol.*, 2001, **35**, 3495.
33 J. Luster, T. Lloyd and G. Sposito, *Environ. Sci. Technol.*, 1996, **30**, 1565.
34 P. Lubal, D. Fetsch, D. Siroky, M. Lubalova, J. Senkyr and J. Havel, *Talanta*, 2000, **51**, 977.
35 P. M. Shanbhag and G. R. Choppin, *J. Inorg. Nucl. Chem.*, 1981, **43**, 3369.
36 B. Gu, H. Yan, P. Zhou, D. B. Watson, M. Park and J. Istok, *Environ. Sci. Technol.*, 2005, **39**, 5268.
37 K. Schmeide, S. Sachs, M. Bubner, T. Reich, K. H. Heise and G. Bernhard, *Inorg. Chim. Acta*, 2003, **351**, 133.
38 S. Tsushima, S. Nagasaki, S. Tanaka and A. Suzuki, *Czech. J. Phys.*, 1999, **49**, 783.
39 S. A. Wood, *Ore Geol. Rev.*, 1996, **11**, 1.
40 D. Zhao, S. Yang, S. Chen, Z. Guo and X. Yang, *J. Radioanal. Nucl. Chem.*, 2011, **287**, 557.
41 F. Schlosser, S. Kruger and N. Rösch, *Inorg. Chem.*, 2006, **24**, 1480.
42 R. S. Ray, S. Kruger and N. Rösch, *Dalton Trans.*, 2009, 3590.
43 O. Zakharieva, A. Kremleva, S. Kruger and N. Rösch, *Int. J. Quantum Chem.*, 2010, **111**, 2045.
44 A. Kremleva, S. Kruger and N. Rösch, *Inorg. Chim. Acta*, 2009, **362**, 2542.
45 C. C. Trout and J. D. Kubicki, *Geochim. Cosmochim. Acta*, 2006, **70**, 44.

46 R. A. Alvarez-Puebla, C. Valenzuela-Calahorro and J. Garrido, *Sci. Total Environ.*, 2006, **358**, 243.
47 T. C. Ramalho, E. F. F. da Cunha, R. B. de Alencastro and A. Espinola, *Water, Air, Soil Pollut.*, 2007, **183**, 467.
48 C. C. Trout and J. D. Kubicki, *Geochim. Cosmochim. Acta*, 2007, **71**, 3859.
49 J. P. Austin, M. Sundararajan, M. A. Vincent and I. H. Hillier, *Dalton Trans.*, 2009, 5902.
50 J. P. Austin, N. A. Burton, I. H. Hillier, M. Sundararajan and M. A. Vincent, *Phys. Chem. Chem. Phys.*, 2009, **11**, 1143.
51 E. A. Nantsis and W. R. Carper, *THEOCHEM*, 1998, **423**, 203.
52 A. Matynia, T. Lenoir, B. Causse, L. Spadini, T. Jacquet and A. Manceau, *Geochim. Cosmochim. Acta*, 2010, **74**, 1836.
53 M. Buhl and H. Kabrede, *J. Chem. Theory Comput.*, 2006, **2**, 1282.
54 M. Sundararajan, A. J. Campbell and I. H. Hillier, *J. Phys. Chem. A*, 2008, **112**, 4451.
55 A. D. Becke, *Phys. Rev. A: At., Mol., Opt. Phys.*, 1988, **38**, 3098.
56 J. P. Perdew, *Phys. Rev. B*, 1986, **33**, 8822.
57 A. Schäfer, H. Horn and R. Ahlrichs, *J. Chem. Phys.*, 1992, **97**, 2571.
58 A. D. Becke, *J. Chem. Phys.*, 1993, **98**, 5648.
59 C. Lee, W. Yang and R. G. Parr, *Phys. Rev. B*, 1988, **37**, 785.
60 A. Schäfer, C. Huber and R. Ahlrichs, *J. Chem. Phys.*, 1994, **100**, 5829.
61 F. Weigend and R. Ahlrichs, *Phys. Chem. Chem. Phys.*, 2005, **7**, 3297.
62 TURBOMOLE V6.0 2009, a development of University of Karlsruhe and Forschungszentrum Karlsruhe GmbH, 1989-2007, TURBOMOLE GmbH, since 2007; available from http://www.turbomole.com.
63 Y. Zhao and D. G. Truhlar, *Theor. Chem. Acc.*, 2008, **120**, 215.
64 M. J. Frisch, G. W. Trucks, H. B. Schlegel, G. E. Scuseria, M. A. Robb, J. R. Cheeseman, G. Scalmani, V. Barone, B. Mennucci, G. A. Petersson, H. Nakatsuji, M. Caricato, X. Li, H. P. Hratchian, A. F. Izmaylov, J. Bloino, G. Zheng, J. L. Sonnenberg, M. Hada, M. Ehara, K. Toyota, R. Fukuda, J. Hasegawa, M. Ishida, T. Nakajima, Y. Honda, O. Kitao, H. Nakai, T. Vreven, J. A. Montgomery, Jr, J. E. Peralta, F. Ogliaro, M. Bearpark, J. J. Heyd, E. Brothers, K. N. Kudin, V. N. Staroverov, R. Kobayashi, J. Normand, K. Raghavachari, A. Rendell, J. C. Burant, S. S. Iyengar, J. Tomasi, M. Cossi, N. Rega, J. M. Millam, M. Klene, J. E. Knox, J. B. Cross, V. Bakken, C. Adamo, J. Jaramillo, R. Gomperts, R. E. Stratmann, O. Yazyev, A. J. Austin, R. Cammi, C. Pomelli, J. W. Ochterski, R. L. Martin, K. Morokuma, V. G. Zakrzewski, G. A. Voth, P. Salvador, J. J. Dannenberg, S. Dapprich, A. D. Daniels, Ö. Farkas, J. B. Foresman, J. V. Ortiz, J. Cioslowski and D. J. Fox, *Gaussian 09, Revision A.1*, Gaussian, Inc., Wallingford, CT, 2009.
65 W. L. Jorgensen and J. Tirado-Rives, *J. Am. Chem. Soc.*, 1988, **110**, 1657.
66 G. A. Kaminski, R. A. Friesner, J. Tirado-Rives and W. L. Jorgensen, *J. Phys. Chem. B*, 2001, **105**, 6474.
67 A. W. Schuttelkopf and D. M. F. van Aalten, *Acta Crystallogr., Sect. D: Biol. Crystallogr.*, 2004, **60**, 1355.
68 C. M. Breneman and K. B. Wiberg, *J. Comput. Chem.*, 1990, **11**, 361.
69 F. Neese, *ORCA, an ab initio density functional and semiempirical program package*, 2009.
70 B. Hess, C. Kutzner, D. van der Spoel and E. Lindahl, *J. Chem. Theory Comput.*, 2008, **4**, 435.
71 J. Wiebke, A. Moritz, M. Glorious, H. Moll, G. Bernhard and M. Dolg, *Inorg. Chem.*, 2008, **47**, 3150.
72 E. A. Ghabbour, M. Shaker, A. El-Toukhy, I. M. Abid and G. Davies, *Chemosphere*, 2006, **64**, 826.
73 MOPAC2009, J. J. P. Stewart, Stewart Computational Chemistry, Colorado Springs, CO, USA, http://openmopac.net, 2008.
74 M. A. Denecke, T. Reich, S. Pompe, M. Bubner, K. H. Heise, H. Nitsche, P. G. Allen, J. J. Butcher, N. M. Edelstein and D. K. Shuh, *J. Phys. IV*, 1997, **7**(C2), 637.
75 M. A. Denecke, S. Pompe, T. Reich, H. Moll, M. Bubner, K. H. Heise, R. Nicolai and H. Nitsche, *Radiochim. Acta*, 1997, **79**, 637.


 